Electronic Supplementary Material (ESI) for RSC Advances.

Supporting Information:

Enhancing the Efficiency of the Hydrogen Evolution Reaction Utilising Fe_3P bulk Modified Screen-Printed Electrodes via the Application of a Magnetic Field

Jack P. Hughes,[1,2] Samuel J. Rowley-Neale[1,2*] and Craig E. Banks[1,2*]

[1]: Faculty of Science and Engineering, Manchester Metropolitan University, Chester Street, Manchester M1 5GD, UK.

[2]: Manchester Fuel Cell Innovation Centre, Manchester Metropolitan University, Chester Street, Manchester M1 5GD, UK.

*To whom correspondence should be addressed.
Email: c.banks@mmu.ac.uk; Tel: ++(0)1612471196; Fax: ++(0)1612476831

Iron Phosphide Screen-Printed Electrode (SPE) Production

The initial working electrodes were incorporated with Fe_2P and Fe_3P internally using specialised stencil screens within the DEK 248 screen-printing unit. (DEK, Weymouth, UK). The incorporation of the Fe_2P and Fe_3P electrocatalytic inks started with the printing of a carbon-graphite ink (product code: C2130814D2; Sun Chemical, U.K.) layer onto a polyester (Autostat, 250 μm thickness) substrate. The layer was then cured at 60ºC for 30 minutes in a fan oven. The connections were sealed with a dielectric paste (product code: D2070423D5; Gwent Electronic Materials Ltd., U.K.) and the unmodified electrodes were ready to use after curing at 60ºC for 30 minutes. Incorporation of the Fe_2P and Fe_3P powder into a carbon-graphitic ink was carried out using weight percentage of M_P to M_I, where M_P is the mass of particulate (the mass of Fe_xP) and M_I is the total mass of the ink including the base graphitic ink, Nafion® solution and the mass of the particulate. Therefore the equation $(M_P/M_I)\times100$ was used to formulate four ink compositions for Fe_xP in the weight percentage range 5, 10, 20 and 40%. The Nafion® solution makes up 10% weight of M_I. The Nafion® solution was reduced to 30% of its initial volume on a hot plate to evaporate water and lower aliphatic alcohols before incorporating into the screen-printing ink.[1] The ink formulations were ultra-sonicated for 30 minutes prior to printing to agitate and disperse the ball milled Fe_3P powders. The 20% Fe_3P-SPEs were the most active towards the HER therefore it was decided to increase the achievable current density of the SPEs by ball milling the Fe3P powder. The powder was milled in a Retsch PM 100 planetary ball mill in the time intervals: 5, 10, 20 and 50 hr in a 50 mL zirconium oxide (ZrO_2) grinding jar (Retsch, Germany) with 2 mm yttrium stabilized zirconia beads (Retsch, Germany). The SPE modification process described above was then repeated using the ball milled Fe_3P powders.

Physicochemical characterisation equipment

The absorption spectra was analysed using the UV-Visible ChemStation software. Scanning electron microscope (SEM) images and surface element analysis were obtained using a JEOL JSM-5600LV model SEM equipped with an energy-dispersive X-ray microanalysis (EDX) package. Raman Spectroscopy was performed using a 'Renishaw InVia' spectrometer equipped with a confocal microscope (×50 objective) and an argon laser (514.3 nm excitation). Measurements were performed at a very low laser power level (0.8 mW) to avoid any heating effects. X-ray diffraction (XRD) was performed using an "X'pert powder PANalytical" model with a copper source of Kα radiation (of 1.54 Å) and Kβ radiation (of 1.39 Å), using a thin sheet of nickel with an absorption edge of 1.49 Å to absorb Kβ radiation. A reflection transmission spinner stage (15 rpm) was implemented to hold the commercially sourced Fe_3P powder. The range was set between 10 and 100 2θ in correspondence with literature ranges.1 Additionally, to ensure well defined peaks an exposure of 50 seconds per 2θ step was implemented with a size of 0.013°. The X-ray photoelectron spectroscopy (XPS) data was acquired using a bespoke ultra-high vacuum system fitted with a Specs GmbH Focus 500 monochromated Al Kα X-ray source, Specs GmbH Phoibos 150 mm mean radius hemispherical analyser with 9-channeltron detection, and a Specs GmbH FG20 charge neutralising electron gun.2 Survey spectra were acquired over the binding energy range 1100 – 0 eV using a pass energy of 50 eV and high resolution scans were made over the C 1s and O 1s lines using a pass energy of 20 eV. Under these conditions the full width at half maximum of the Ag 3d5/2 reference line is ca. 0.7 eV. In each case, the analysis was an area-average over a region approximately 1.4 mm in diameter on the sample surface, using the 7 mm diameter aperture and lens magnification of ×5. The energy scale of the instrument is calibrated according to ISO 15472, and the intensity scale is calibrated using an in-house method traceable to the UK National Physical Laboratory. Data were quantified using Scofield cross sections corrected for the energy dependencies of the electron attenuation lengths and the instrument transmission. Data interpretation was carried out using CasaXPS software v2.3.16.

Table T1. Summary of values relating to the electrochemical experiments carried out with the Fe_3P $SPE_{20h\,BM}$ in the presence of a perpendicular magnetic field (B –). The distance of the magnets from the electrode surface is represented by z (mm), the magnetic flux density is represented by B (T) and the Lorentz force density is represented by F (N cm^{-3}).

z (mm)	B (T)	F (N cm^{-3})	Applied voltage required to reach – 10 mA cm^{-2} (V vs. RHE)	Observed current density (mA cm^{-2})
5	0.29	0.0057	-0.77	-19.59
10	0.33	0.00682	-0.74	-20.68
20	0.16	0.0028	-0.82	-17.82
40	0.04	0.00079	-0.84	-17.71

Figure S1. SEM imaging (A) and EDX elemental mapping analysis (B) of raw and ball milled Fe_3P powders, scale bar 1-50 µm. (1) raw (2) 5 hr (3) 10 hr (4) 20 hr and (5) 50 hr.

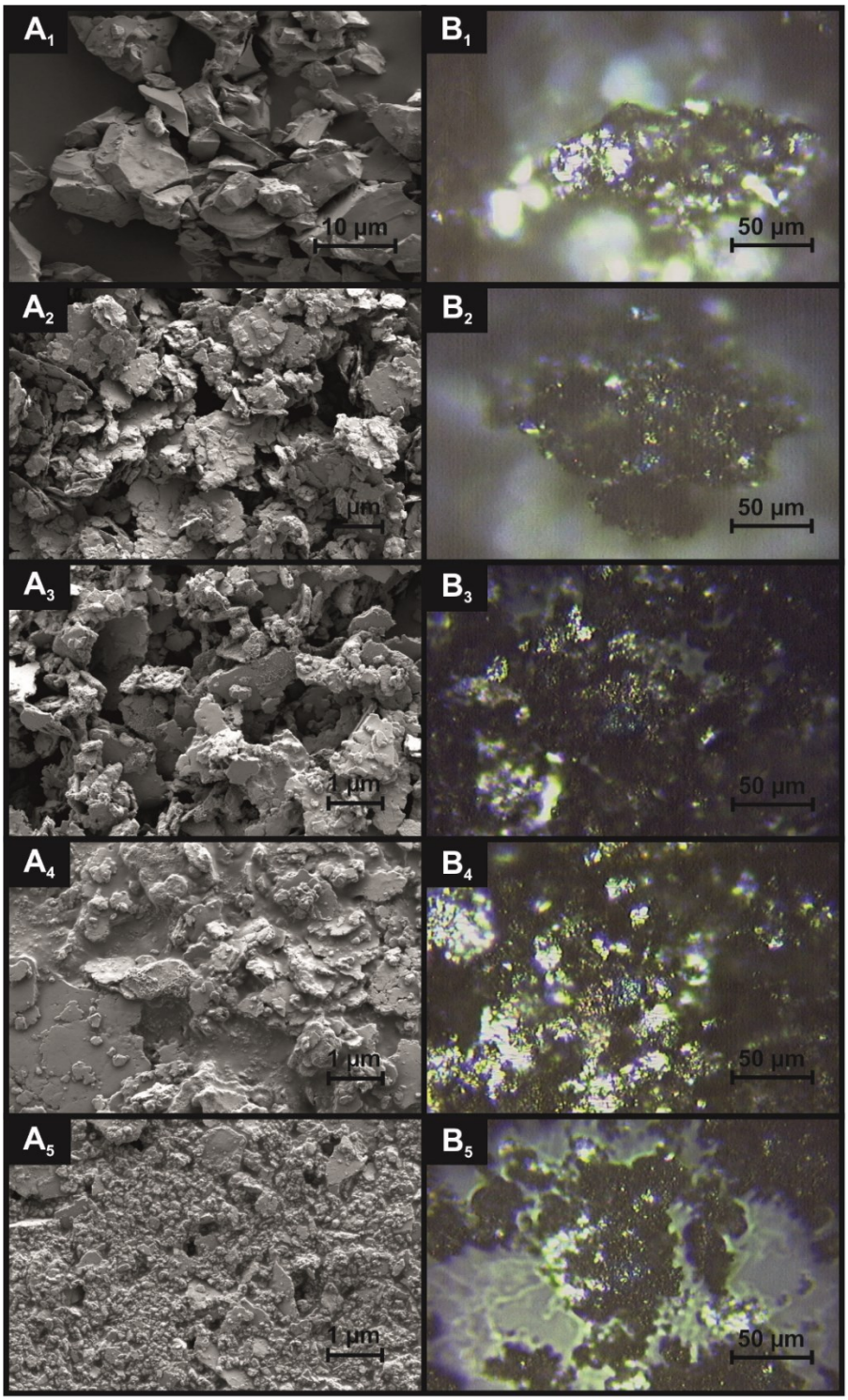

Table T2. EDX elemental analysis of the raw and ball milled Fe_3P powder.

Ball milling duration (hr)	Element	Weight (%)
0	C	3.3
	O	3.5
	Fe	82.2
	P	11.0
5	C	3.6
	O	4.9
	Fe	79.0
	P	12.5
10	C	5.0
	O	5.6
	Fe	76.9
	P	12.5
20	C	11.8
	O	7.1
	Fe	69.1
	P	12.0
50	C	7.1
	O	11.5
	Fe	67.9
	P	13.5

Figure S2. XRD analysis of raw and ball milled Fe_3P powders. (A) raw (B) 5 hr (C) 10 hr (D) 20

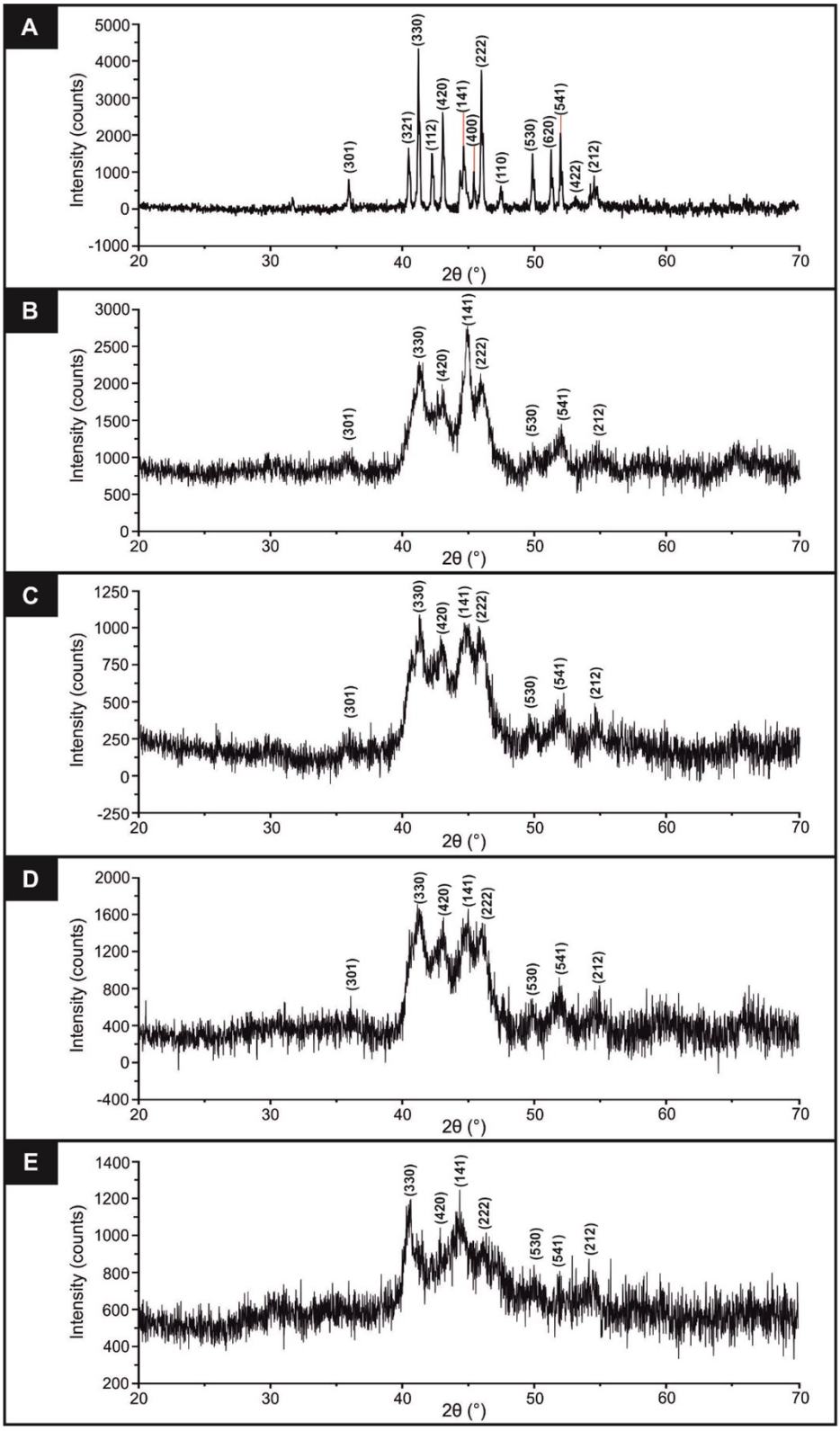

hr and (E) 50 hr.

Figure S3. Raman spectra of the raw and ball milled Fe_3P powders deposited onto a silicon wafer between 100 and 2000 cm^{-1}. (A) raw (B) 5 hr (C) 10 hr (D) 20 hr and (E) 50 hr.

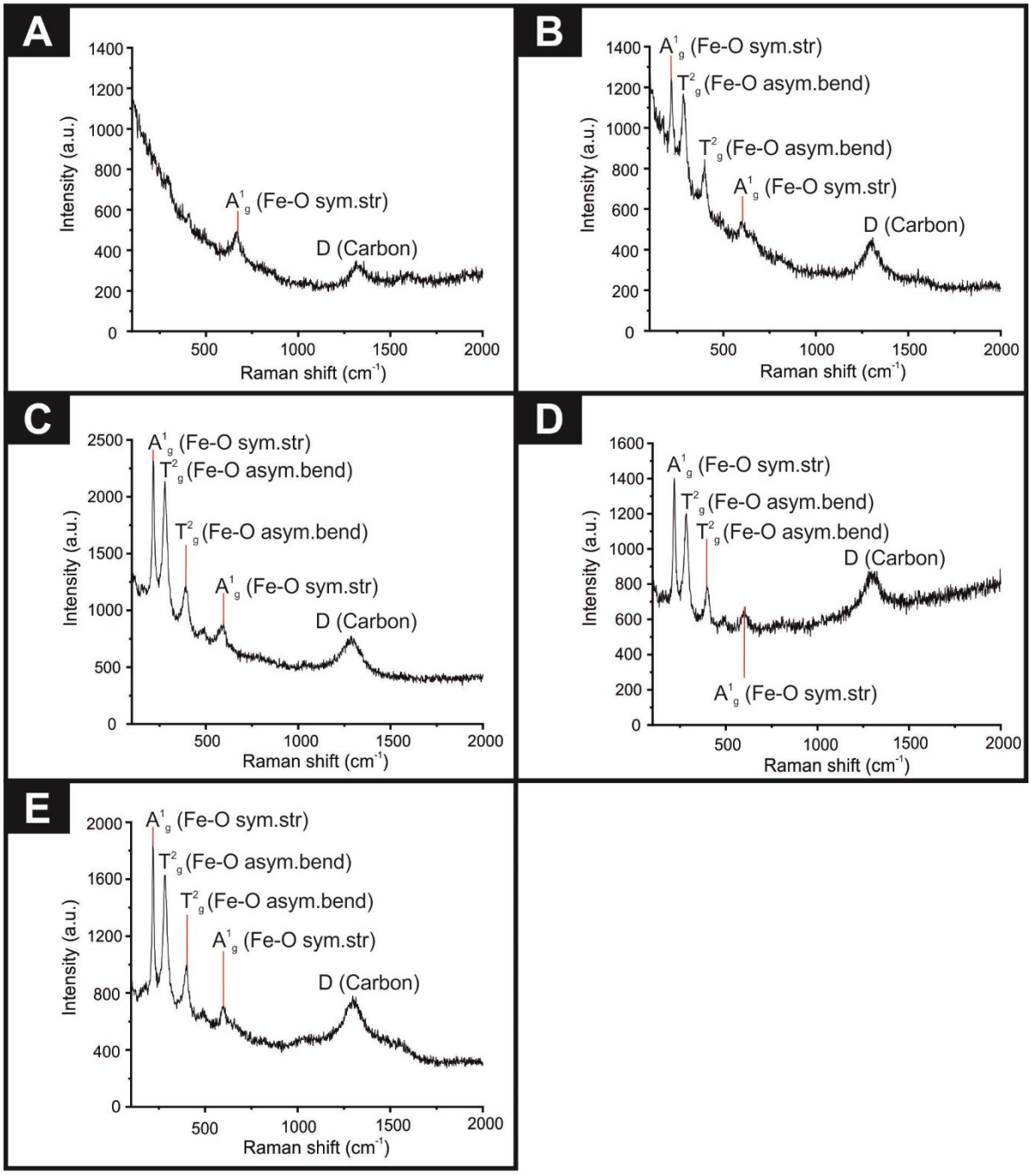

Figure S4. XPS spectra of (A) Fe $2p_{3/2}$ and $2p_{1/2}$ (B) P 2p peaks of raw and ball milled Fe_3P powders deposited onto a silicon wafer between 100 and 2000 cm^{-1}. (1) raw (2) 5 hr (3) 10 hr (4)

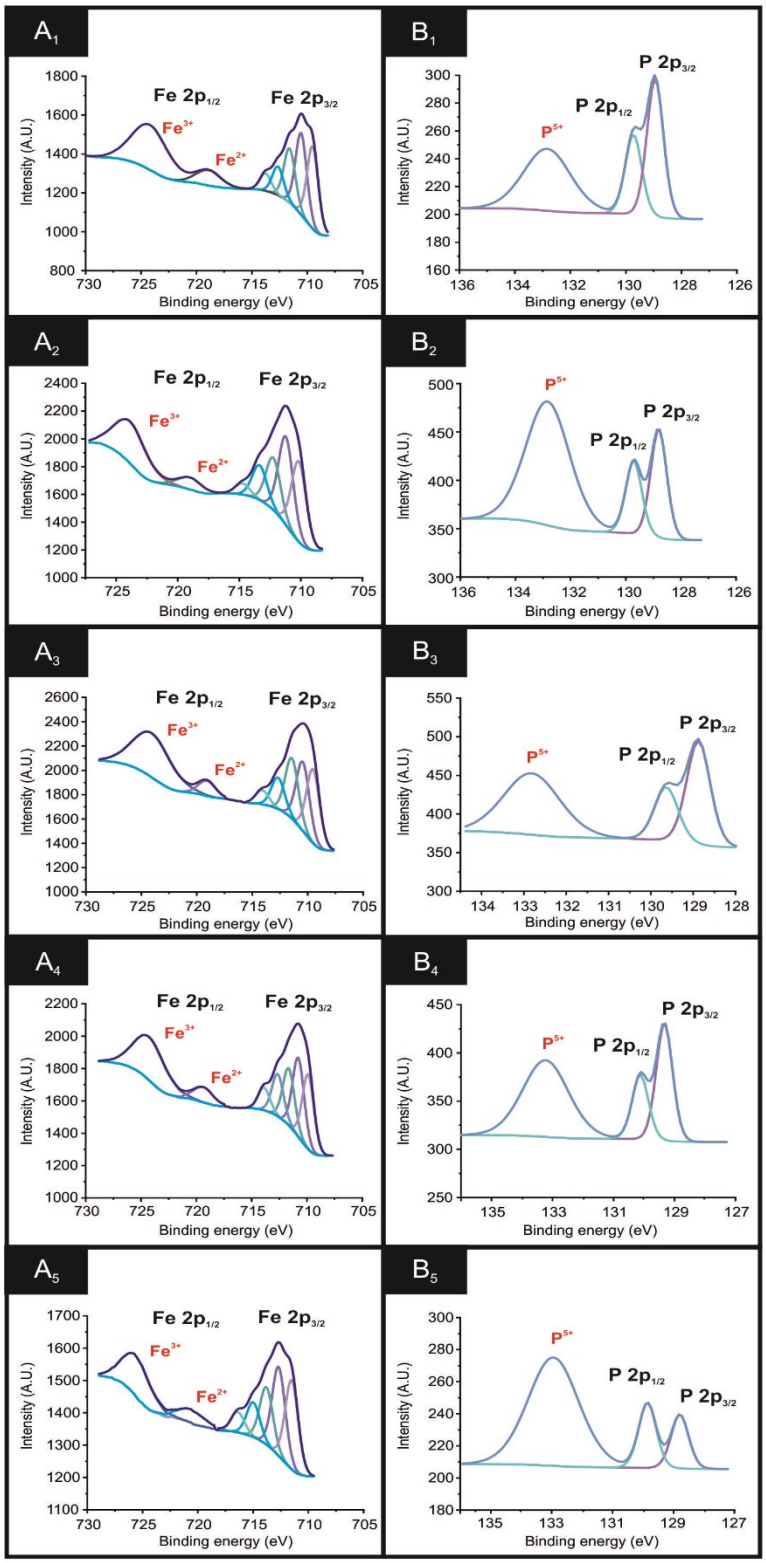

20 hr and (5) 50 hr.

Figure S5. Chronoamperometry utilising the Fe_3P $SPE_{20h\ BM}$ at −0.50 V (*vs*. RHE) for a duration of 24 hrs in 0.5 M H_2SO_4, in the presence of a magnetic field (B = 0.33 T).

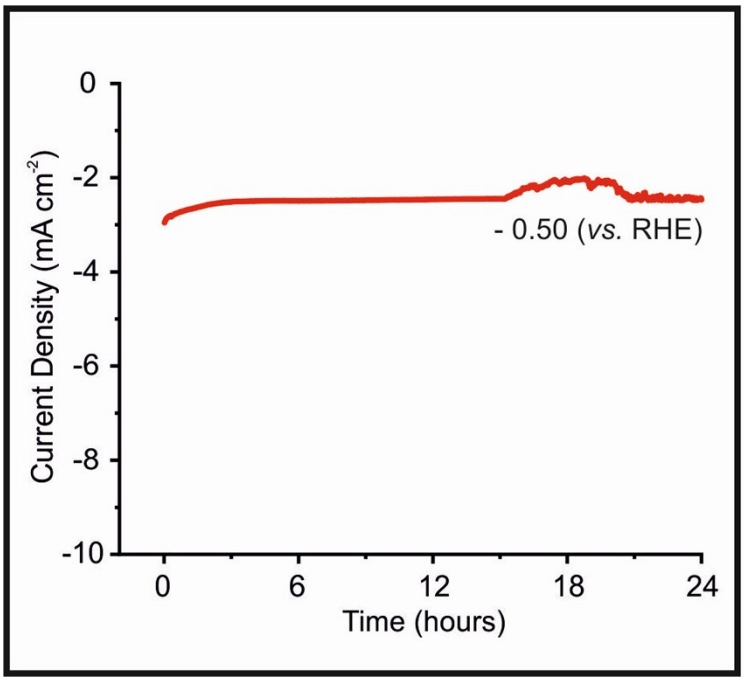

Specific Activity, *SA*

Specific activities, *SA*, were calculated according to a method by Chaiburi *et al.*[2] using the following equation: $SA = \frac{I_p}{ECSA}$, where I_p is the peak current (A) exhibited by each Fe_3P SPE and *ECSA* is the electrochemically derived active surface area of each Fe_3P SPE (cm^{-2}). The specific activity is calculated as a function of the peak current (A) and the electroactive working area (cm^2) of the ball milled Fe_3P SPE variants as follows:

$$SA_{Fe_3P\ in\ Fe_3P\ SPE_{5h\ BM}} = \frac{0.0177\ A}{0.059\ cm^2} = 0.296\ A\ cm^{-2}$$

$$SA_{Fe_3P\ in\ Fe_3P\ SPE_{10h\ BM}} = \frac{0.0178\ A}{0.062\ cm^2} = 0.297\ A\ cm^{-2}$$

$$SA_{Fe_3P\ in\ Fe_3P\ SPE_{20h\ BM}} = \frac{0.0207\ A}{0.066\ cm^2} = 0.314\ A\ cm^{-2}$$

$$SA_{Fe_3P\ in\ Fe_3P\ SPE_{50h\ BM}} = \frac{0.0196\ A}{0.064\ cm^2} = 0.306\ A\ cm^{-2}$$

Hydrogen Turnover Frequency, ToF

The effect of a magnetic field on the electrochemical activity of the Fe_3P $SPE_{20h\,BM}$ 'per active site' was carried out using methodology reported by *Benck et al .*[3] and *Laursen et al.* [4].

The total number of hydrogen turnovers was calculated using the value of current density (10 mA cm^{-2}), at a 25 mV s^{-1} scan rate, utilising the following formula:

$$j\left(\frac{mA}{cm^2}\right)\left(\frac{1\ A}{1000mA}\right)\left(\frac{1C\ s^{-1}}{1\ A}\right)\left(\frac{1\ mol\ e^-}{96485.3\ C}\right)\left(\frac{1\ mol\ H_2}{2\ mol\ e^-}\right)\left(\frac{6.02214\times10^{23}}{1\ mol\ H_2}\right) = 3.12\times10^{15}\frac{H_2\ s^{-1}}{cm^2}\ per\ \frac{mA}{cm^2}$$

[1]

The number of active surface sites of Fe_3P per cm^2 geometric area is then calculated from the following equations:

$$V_m = \frac{M}{\rho} = \frac{198.51\ g\ mol^{-1}}{6.74\ g\ cm^{-3}} = 29.45\ \frac{cm^3}{mol(Fe_3P)} \qquad [2]$$

where V_m is the molar volume of the tetragonal unit cell of Fe_3P, M is the molar mass of Fe_3P and ρ is the mass density of Fe_3P. Each formula unit contains 4 atoms of Fe and P, therefore the number of active surface sites of Fe_3P per cm^2 geometric area is calculated as follows:

$$\#Active\ sites\ (Fe_3P) = \left(\frac{4\ atoms\ per\ formula\ unit}{\frac{29.45\ cm^3\ mol\ (Fe_3P)^{-1}}{6.0221\times10^{23}mol^{-1}}}\right)^{\frac{2}{3}} = 8.17\times10^{22}\ active\ sites\ cm^2 \qquad [3]$$

Hydrogen turnover frequency (ToF) is then worked out according to the following equation:

$$ToF\ per\ site = \frac{\#\ Total\ hydrogen\ turnovers\ per\ cm^2\ geometric\ area\ \times|j|}{\#\ Surface\ sites\ (Catalyst)\ per\ cm^2\ geometric\ area\ \times A_{ECSA}} \qquad [4]$$

The electrochemical active surface area (ECSA) of the Fe_3P $SPE_{20h\ BM}$ was calculated as 0.066 cm^2, obtained by carrying out a scan rate study in hexaammineruthenium (III) chloride (RuHex) at the scan rates: 5, 10, 25, 50, 100, 200 and 300 mV S^{-1}.

The ToF of the Fe_3P $SPE_{20h\ BM}$ in the absence of a magnetic field is then calculated using the value of current density (j) at the HER onset potential, shown below:

$$ToF\ (Fe_3P\ SPE_{20h\ BM}) = \frac{(3.12 \times 10^{15}) \frac{H_2\ s^{-1}}{cm^2}\ per\ \frac{mA}{cm^2} \times 0.47\ mA\ cm^{-2}}{8.17 \times 10^{22}\ active\ sites\ per\ cm^2 \times 0.066\ cm^2} = 2.72 \times 10^{-7}\ H_2\ s^{-1}\ per\ active\ site$$

The ToF of the Fe_3P $SPE_{20h\ BM}$ in the presence of magnetic fields of differing magnetic flux densities is calculated using the value of j at the HER onset potential, shown below. (Note: the ECSA is kept constant throughout the calculations).

$$ToF\ (Fe_3P\ SPE_{20h\ BM})\ in\ 0.04\ T = \frac{(3.12 \times 10^{15}) \frac{H_2\ s^{-1}}{cm^2}\ per\ \frac{mA}{cm^2} \times 0.57\ mA\ cm^{-2}}{8.17 \times 10^{22}\ active\ sites\ per\ cm^2 \times 0.066\ cm^2} = 3.30 \times 10^{-7}\ H_2\ s^{-1}\ per\ active\ site$$

$$ToF\ (Fe_3P\ SPE_{20h\ BM})\ in\ 0.16\ T = \frac{(3.12 \times 10^{15}) \frac{H_2\ s^{-1}}{cm^2}\ per\ \frac{mA}{cm^2} \times 0.72\ mA\ cm^{-2}}{8.17 \times 10^{22}\ active\ sites\ per\ cm^2 \times 0.066\ cm^2} = 4.17 \times 10^{-7}\ H_2\ s^{-1}\ per\ active\ site$$

$$ToF\ (Fe_3P\ SPE_{20h\ BM})\ in\ 0.33\ T = \frac{(3.12 \times 10^{15}) \frac{H_2\ s^{-1}}{cm^2}\ per\ \frac{mA}{cm^2} \times 0.98\ mA\ cm^{-2}}{8.17 \times 10^{22}\ active\ sites\ per\ cm^2 \times 0.066\ cm^2} = 5.67 \times 10^{-7}\ H_2\ s^{-1}\ per\ active\ site$$

$$ToF\ (Fe_3P\ SPE_{20h\ BM})\ in\ 0.29\ T = \frac{(3.12 \times 10^{15}) \frac{H_2\ s^{-1}}{cm^2}\ per\ \frac{mA}{cm^2} \times 0.97\ mA\ cm^{-2}}{8.17 \times 10^{22}\ active\ sites\ per\ cm^2 \times 0.066\ cm^2} = 5.61 \times 10^{-7}\ H_2\ s^{-1}\ per\ active\ site$$

Magnetic Flux Density, *B*

The magnetic flux densities (*B*) at each distance (z) from the electrode, reported in Table S3, are calculated through the following equation on the symmetry axis of an axially magnetised ring magnet:

$$B = \frac{B_r}{2}\left[\frac{D+z}{\sqrt{R_a^2+(D+z)^2}} - \frac{z}{\sqrt{R_a^2+z^2}} - \left(\frac{D+z}{\sqrt{R_i^2+(D+z)^2}} - \frac{z}{\sqrt{R_i^2+z^2}}\right)\right] \quad [1]$$

where B_r is the Remanence field, independent of the magnet's geometry, for a grade N42 ring magnet, obtained from physical magnet data) [5], D is the thickness (or height) of the magnet ring, z is the distance from the magnetic Fe_3P $SPE_{20h\ BM}$ to the magnet, R_a is the outside radius of the ring and R_i is the inside radius of the ring. The obtained values for B are achieved by controlling

the distance of the magnet from the electrode surface. The Lorentz force density or F (N cm^{-3}) can then be calculated from the equation below:

$$F = j \times B \quad [2]$$

where j is the voltammetric peak current density (A cm^{-2}) of the Fe_3P $SPE_{20h\ BM}$ at each varied magnetic flux density.

Table T3. Summary of current literature regarding transition metal phosphides HER electrocatalysts.

Catalyst	Supporting electrode	Electrolyte	Stability in acidic media	Deposition technique	Loading	HER onset (V)	Current Density at 150mV (mA/cm^{-2})	Tafel value (mV dec^{-1})	Ref
Fe-WO$_X$P/rGO	GC	0.5 M H_2SO_4	8h at −10 mA cm^{-2}	Drop casting	-	−0.075 (*vs.* RHE)	−74	41.9	6
CoPS/N-S	GC	0.5 M H_2SO_4	16h at 80mV (*vs.* RHE)	Drop casting	0.17 mg cm^{-2}	−0.045 (*vs.* RHE)	−10	68	7
$Co_{0.59}Fe_{0.41}P$	GC	0.5 M H_2SO_4	20h at 72mV (vs. RHE)	Drop casting	0.35 mg cm^{-2}	−0.03 (*vs.* RHE)	−38	52	8
Ni_2P–CoP	GC	0.5 M H_2SO_4	14h at 0.14 V (vs. RHE)	Drop casting	0.357 mg cm^{-2}	−0.06 (*vs.* RHE)	−71	64	9
CoP CPHs	GC	0.5 M H_2SO_4	>12h at 130 mV (vs. RHE)	Drop casting	0.35 mg cm^{-2}	−0.06 (*vs.* RHE)	−17	51	10
CP@Ni-P	CF	0.5 M H_2SO_4	150h at −10 mA cm^{-2} (vs. RHE)	Chemical synthesis	0.30 mg cm^{-2}	−0.05 (*vs.* RHE)	−20	58.8	11
Ni_2P	GC	0.5 M H_2SO_4	500 cycles (0 to −0.25 V) (vs. RHE)	Drop casting	-	−0.03 (*vs.* RHE)	−14	75	12
Co-P	GC	0.5 M H_2SO_4	13h at −10 mA cm^{-2} (vs. RHE)	Drop casting	0.20 mg cm^{-2}	−0.04 (*vs.* RHE)	−8	56	13
Fe_2P	FTO	0.5 M H_2SO_4	20h at 120 mV (vs. RHE)	CVD	-	−0.05 (*vs.* RHE)	−76	66	14
Fe_3P	FTO	0.5 M H_2SO_4	20h at 120 mV (vs. RHE)	CVD	-	−0.02 (*vs.* RHE)	-	57	14
FeP	GC	0.5 M H_2SO_4	60h at −50 mA cm^{-2} (vs. RHE)	Drop casting	0.28 mg cm^{-2}	−0.025 (*vs.* RHE)	−91	57	15
FeP NSs	GC	0.5 M H_2SO_4	-	Drop casting	0.28 mg cm^{-2}	−0.09 (*vs.* RHE)	−4	67	16
Fe_2P NPs	Ti foil	0.5 M H_2SO_4	0.5h at −10 mA cm^{-2} (vs. RHE)	Drop casting	0.11 mg cm^{-2}	–0.09 (*vs.* RHE)	*Ca.* −26	64	17
FeP/CN	GC	0.5 M H_2SO_4	24h at 140 mV (vs. RHE)	Drop casting	1 mg cm^{-2}	*Ca.* –0.04 (*vs.* RHE)	-	65	18
FeP NRs	GC	0.5 M H_2SO_4	40h at 200 mV (vs. RHE)	Drop casting	0.2 mg cm^{-2}	–0.11 (*vs.* RHE)	*Ca.* −25	55	19
FeP/C NCs	GC	0.5 M H_2SO_4	16h at −2 mA cm^{-2} (vs. RHE)	Drop casting	0.34 mg cm^{-2}	−0.06 (*vs.* RHE)		56	20
Fe_2P	SPE	0.5 M H_2SO_4	-	Screen-printing	20%	−0.19 (*vs.* RHE)	-	-	This work
Fe_3P	SPE	0.5 M H_2SO_4		Screen-printing	20%	−0.11 (*vs.* RHE)	-0.68	88.5	This Work

: CPH; concave polyhedron GC; Glassy Carbon RHE; Reversible hydrogen electrode NF; Nickel foam NS: Nanosheet; NP: Nanoparticle A; Activated rGO; Reduced graphene oxide GA; Graphene aerogel CVD; Chemical vapor deposition G; Graphene CF; Carbon filter FTO; Fluorine doped Tin Oxide; CN: Carbon nanosheets NR: Nanorod

References

1. W. Wang, S. Chen, J. Li and W. Wang, *Int. J. Hydrogen Energy*, 2015, **40**, 4649-4658.
2. C. Chaiburi and V. Hacker, *Energy Procedia*, 2017, **138**, 229-234.
3. J.D.Benck, Z.Chen, L.Y.Kuritzky, A.J.Forman and T.F.Jaramillo, *ACS Catal.*, 2012, **2**, 1916-1923.
4. A. B. Laursen, K. R. Patraju, M. J. Whitaker, M. Retuerto, T. Sarkar, N. Yao, K. V. Ramanujachary, M. Greenblatt and G. C. Dismukes, *Energy Environ. Sci.*, 2015, **8**, 1027-1034.
5. Supermagnete, Physical magnet data, https://www.supermagnete.de/eng/physical-magnet-data, (accessed 23/03/2020, 2020).
6. T. H. Wondimu, B. Chen, D. M. Kabtamu, H. Chen, A. W. Bayeh, H. Huang and C. Wang, *Int. J. Hydrogen Energy*, 2018, **43**, 6481-6490.
7. Y. Li, S. Niu, D. Rakov, Y. Wang, M. Cabán-Acevedo, S. Zheng, B. Song and P. Xu, *Nanoscale*, 2018, **10**, 7291-7297.
8. J. Hao, W. Yang, A. Zhang and J. Tang, *Nanoscale*, 2015, **7**, 11055-11062.
9. W. Zhou, J. Lu, K. Zhou, L. Yang, Y. Ke, Z. Tang and S. Chen, *Nano Energy*, 2016, **28**, 143-150.
10. M. Xu, L. Han, Y. Han, Y. Yu, J. Zhai and S. Dong, *J. Mater. Chem. A*, 2015, **3**, 21471-21477.
11. X. Wang, W. Li, D. Xiong, D. Y. Petrovykh and L. Liu, *Adv. Funct. Mater.*, 2016, **26**, 4067-4077.
12. J.-S. Moon, J.-H. Jang, E.-G. Kim, Y.-H. Chung, S. J. Yoo and Y.-K. Lee, *J. Catal.*, 2015, **326**, 92-99.
13. A. Sumboja, T. An, H. Y. Goh, M. Lübke, D. P. Howard, Y. Xu, A. D. Handoko, Y. Zong and Z. Liu, *ACS Appl. Mater. Interfaces*, 2018, **10**, 15673-15680.
14. D. E. Schipper, Z. Zhao, H. Thirumalai, A. P. Leitner, S. L. Donaldson, A. Kumar, F. Qin, Z. Wang, L. C. Grabow, J. Bao and K. H. Whitmire, *Chemistry of Materials*, 2018, **30**, 3588-3598.
15. F. Wang, X. Yang, B. Dong, X. Yu, H. Xue and L. Feng, *Electrochem. Commun.*, 2018, **92**, 33-38.
16. Y. Xu, R. Wu, J. Zhang, Y. Shi and B. Zhang, *Chem. Commun.*, 2013, **49**, 6656-6658.
17. G. Cho, H. Kim, Y. S. Park, Y.-K. Hong and D.-Y. Ha, *Int. J. Hydrogen Energy*, 2018, **43**, 11326-11334.
18. M. H. Suliman, A. Adam, M. N. Siddiqui, Z. H. Yamani and M. Qamar, *Carbon*, 2019, **144**, 764-771.
19. H. Du, S. Gu, R. Liu and C. M. Li, *Int. J. Hydrogen Energy*, 2015, **40**, 14272-14278.
20. Z. Gao, Q. Gao, Z. Liu, C. Zhang, X. Zhang, X. Liu, R. Wang and N. Li, *RSC Adv.*, 2016, **6**, 114430-114435.